Hybrid plasmonic waveguide coupling of photons from a single molecule

S. Grandi ⓘD, M. P. Nielsen ⓘD, J. Cambiasso, S. Boissier, K. D. Major, C. Reardon, T. F. Krauss ⓘD, R. F. Oulton ⓘD, E. A. Hinds, and A. S. Clark ⓘD

View Online   **Export Citation**   **CrossMark**

ARTICLES YOU MAY BE INTERESTED IN

Hybrid plasmonic waveguide coupling of photons from a single molecule

View Online   Export Citation   CrossMark

S. Grandi,[1,a]   M. P. Nielsen,[2,b]   J. Cambiasso,[2]   S. Boissier,[1]   K. D. Major,[1]   C. Reardon,[3]   T. F. Krauss,[3]   R. F. Oulton,[2]   E. A. Hinds,[1]   and A. S. Clark[1,c]

AFFILIATIONS

[1] Centre for Cold Matter, Blackett Laboratory, Prince Consort Road, South Kensington SW7 2AZ, United Kingdom
[2] Experimental Solid State Physics, Blackett Laboratory, Prince Consort Road, South Kensington SW7 2AZ, United Kingdom
[3] Department of Physics, University of York, Heslington, York YO10 5DD, United Kingdom

[a] **Current address:** ICFO-Institut de Ciencies Fotoniques, The Barcelona Institute of Science and Technology, E-08860 Castelldefels (Barcelona), Spain.
[b] **Current address:** School of Photovoltaic and Renewable Energy Engineering, University of New South Wales, Sydney, NSW 2052, Australia.
[c] **Email:** alex.clark@imperial.ac.uk

ABSTRACT

We demonstrate the emission of photons from a single molecule into a hybrid gap plasmon waveguide. Crystals of anthracene, doped with dibenzoterrylene (DBT), are grown on top of the waveguides. We investigate a single DBT molecule coupled to the plasmonic region of one of the guides and determine its in-plane orientation, excited state lifetime, and saturation intensity. The molecule emits light into the guide, which is remotely out-coupled by a grating. The second-order autocorrelation and cross-correlation functions show that the emitter is a single molecule and that the light emerging from the grating comes from that molecule. The coupling efficiency is found to be $\beta_{WG} = 11.6(1.5)\%$. This type of structure is promising for building new functionality into quantum-photonic circuits, where localized regions of strong emitter-guide coupling can be interconnected by low-loss dielectric guides.

I. INTRODUCTION

Despite great advances over the last decade, the wider uptake of quantum technology has been inhibited by the lack of an efficient single photon source. Among several candidates,[1] single molecules are promising as a way to deliver narrow-band photons rapidly and on demand.[2–5] A variety of molecules are photostable and several wavelengths are available by choosing suitable combinations of dopants and hosts.[6] While fulfilling most of the requirements for quantum technologies,[7] molecules naturally emit light into many directions, as do most emitters,[1] and therefore, collection of the photons requires some attention. The use of micropillars has been a very successful approach,[8–10] but is not naturally suited to building optical circuits as the extraction of photons is perpendicular to the chip. Dielectric waveguides can encourage emission into the plane of the chip,[4,11–13] but good coupling requires the emitters to

be placed inside the guide,[14–16] which is a challenge, and even then the coupling is limited by the transverse mode area of the guide. Plasmonic waveguides can have much smaller mode areas, but are compromised by absorption losses and nonradiative decay of the emitter.[17,18] Plasmonic antennas can help by concentrating the field at the site of the emitter into a much smaller volume and can redirect the emission into a well-controlled direction. This idea was demonstrated with a Yagi-Uda antenna,[19,20] but it did not direct the light into a single optical mode and, like the micropillar, is not naturally compatible with a planar integrated architecture. Here, we have taken a hybrid dielectric–metal approach,[21] using a planar hybrid gap plasmon waveguide (HGPW). The propagating hybrid optical mode transitions from mostly dielectric to mostly plasmonic and back to mostly dielectric, coupling to a single molecule of dibenzoterrylene (DBT) in the plasmonic region. Therefore, the small transverse mode area enhances photon emission into the waveguide,

after which the photon moves into the low-loss dielectric region. This structure can provide both high coupling and low loss, making it suitable for an optical network, where single emitters interact with the waveguide field in selected "hot spots," while low-loss propagation interconnects them.

II. HGPW DESIGN, FABRICATION, AND FUNCTIONALIZATION

Our HGPW is based on a design introduced by Lafone et al.[21] and first fabricated and studied by Nielsen et al.[22,23] The design was modified to operate at ~785 nm central emission wavelength of DBT by replacing the silicon and gallium arsenide used in previously fabricated devices[22–24] with titanium dioxide (TiO_2). Figure 1 shows a schematic cross-section of the device, highlighting the underlying structure of a single HGPW. A 300 nm-thick layer of TiO_2 is first deposited on a silica (SiO_2) substrate. Gold gratings deposited on the TiO_2 are covered by an 80 nm spacing layer of SiO_2. Finally, two gold slabs are deposited on top of the SiO_2. The gratings are placed over the TiO_2 layer but underneath the gold slabs and spacer. They couple light in and out of the TiO_2 slab, where it propagates between the gold islands predominantly as a TE mode. There is no dielectric confinement of the mode in the lateral direction, as the TiO_2 layer covers the entire substrate and is shared by all the fabricated devices. However, the field is prevented from spreading in the plane by its coupling to the plasmon. This requires careful adjustment of the thickness of the SiO_2 spacer layer. As the gold islands taper to form a smaller gap, the mode becomes increasingly hybridized with the plasmon mode on the edges of the gold. Figures 1(a) and 1(b) show the distribution of electric field energy density calculated in

COMSOL for channels of two different gap widths, considering a layer of anthracene of 60 nm placed over the structure. In Fig. 1(a), the gold edges are separated by 200 nm and the intensity is concentrated on the edges of the gold. In Fig. 1(b), where the gap is 1000 nm, most of the intensity is in the TiO_2 layer. By controlling the hybridization in this way, it is possible to benefit from the field confinement, while still retaining a long enough propagation length that the field can emerge from the structure and be coupled out the other side. This tradeoff is shown in panels (c) and (d) of Fig. 1, where the energy distribution across the device and the propagation length as a function of channel gap width are plotted. Here, the propagation length is defined by fitting the transmitted power as a function of length x to the curve $A\,e^{-x/\lambda_{prop}}$, where λ_{prop} is the propagation length. It is possible to see that for gap widths smaller than 300 nm, the field is extracted from the TiO_2 layer and is progressively concentrated in the gap region. This is accompanied by a decrease in propagation length, as the mode area is reduced.

Figure 2(a) shows a scanning electron microscope image of four HGPWs, where the plasmonic regions vary in length from 0 to 6 μm. Individual DBT molecules were deposited on top of our HGPW devices using a recently developed method.[12] A 1 mMol solution of DBT in toluene was diluted in diethyl ether at a volume ratio of 1:2000 and spin-coated onto our sample. A glass vial was filled with 2 g of finely ground anthracene powder and heated to 240 °C on a hotplate inside a glove box, purged of oxygen and filled with nitrogen gas to decrease the chance of the molecules photobleaching.[25] The vial was covered with a glass microscope cover slip. After roughly 2 min, the cover slip was removed and the HGPW chip was put in its place. A growth time of about 2 min provided the desired coverage
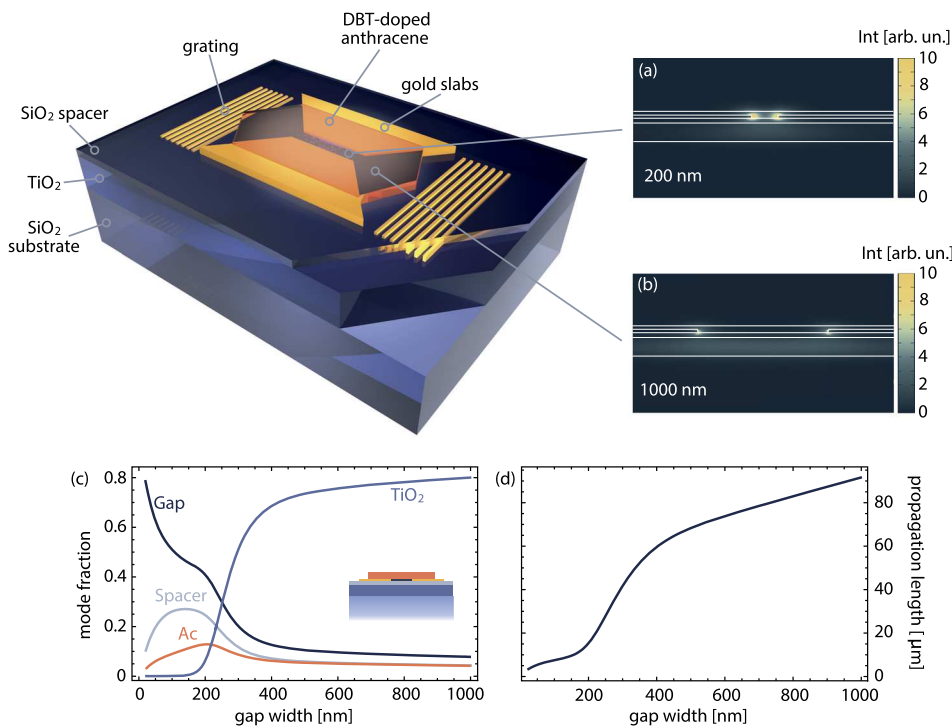
FIG. 1. Schematic of the HGPW showing the layer structure, including a hexagonal DBT-doped anthracene crystal on the top. The two insets show the calculated intensity profiles of light in the HGPW for a gold gap of (a) 200 nm and (b) 1000 nm. (c) Distribution of the mode energy across the layers, as a function of channel gap width. The inset shows the various areas of the device considered. Although the gap is also filled with DBT-doped anthracene, it is shown in dark blue as the field is considered separately from the rest of the anthracene crystal. (d) Propagation length of the hybrid mode, again as a function of channel gap width.
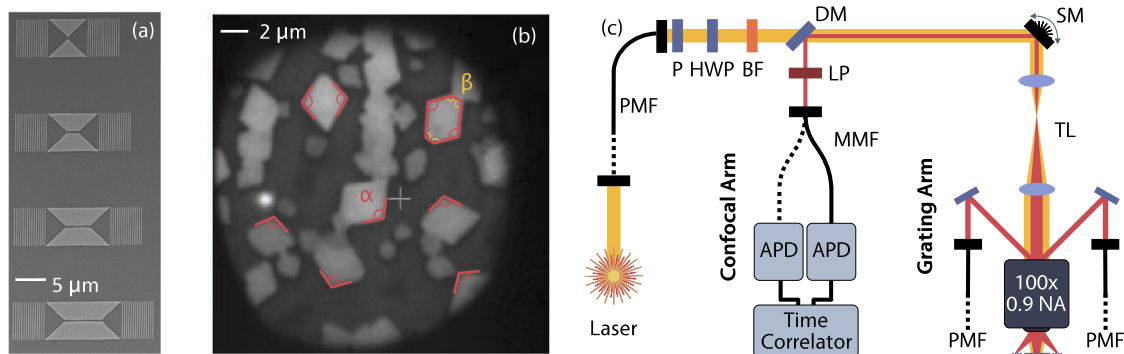
FIG. 2. (a) SEM image of four HGPWs whose plasmonic regions vary in length from 0 to 6 μm. (b) White light image of anthracene crystals grown from supersaturated vapor. The angles α = 109° and β = 125° are as expected for bulk crystals. (c) Schematic of the confocal microscope used to study coupling of single molecules to hybrid plasmonic waveguides. PMF: polarization-maintaining fiber; P: polarizer; HWP: half-wave plate; BF: band-pass filter; DM: dichroic mirror; SM: steering mirrors; TL: telescopic lenses; LP: long-pass filter; MMF: multimode fiber; APD: avalanche photodiode.

of anthracene crystals. This growth time results in crystals which are less than 100 nm thick. Figure 2(b) shows a white light microscope image of the crystals, with the angles α and β being those expected for anthracene.[26] The anthracene crystals stabilize DBT emission, such that it can be treated as a pseudo-two-level system.[12] Moreover, the anthracene crystal prevents bleaching by excluding oxygen and suppresses the intersystem crossing probability to the molecular triplet state[2] to be below 10^{-7}.

The confocal microscope used to study the waveguides is presented in Fig. 2(c). A laser provided excitation light—either a cw external cavity diode laser (Toptica) at 780 nm wavelength or a pulsed diode laser (PicoQuant) at 781 nm. The laser light was cleaned in mode, polarization, and spectrum, then directed to a microscope objective (Nikon ApoPlan Fluo, 100x, 0.9 NA). A telecentric system of lenses and a set of two galvo mirrors allowed raster scanning of the focused laser spot across the sample. The resulting fluorescence was separated from the pump light by a dichroic mirror (Semrock) and further filtered by two 800 nm long-pass filters before being detected. A pellicle beam splitter was placed before the objective to add two additional beam paths, allowing us to couple light in and out of the gratings (for a more detailed setup, see supplementary material Fig. S1). These paths could be connected to the excitation laser to measure transmission loss through the device, or to single-photon detectors to estimate the coupling efficiency. In the latter case, a 792 nm filter was placed before the fiber coupling.

III. RESULTS AND DISCUSSION

The HGPW of interest, shown in Fig. 3(a), is 200 nm wide at the center of the tapered region. We chose to work with this short HGPW as it has the lowest propagation loss. For coupling to longer HGPWs with higher loss, see supplementary material, Fig. S3. Figure 3(b) shows fluorescence from the dashed box area, obtained by a confocal scan using cw light at 780 nm. It should be noted that only one molecule seen in this confocal microscope scan resulted in photon detection events from a grating output. The signal from that DBT molecule, found near the center of this device, is indicated by the red dashed circle. We first checked the orientation of

this molecule by varying the polarization of the excitation light while monitoring the detected photon rate, as reported in Fig. 3(c). This showed that the optical dipole was only 6° $\pm$ 2° away from the optimum, this being perpendicular to the direction of propagation. We then varied the intensity of the excitation light while collecting fluorescence, both from the site of the molecule and from the grating to the left in Fig. 3(a). In both collection arms, the fluorescence rate saturates, as shown in Fig. 3(d). The data points are well modeled by the saturation function

$$R = R_\infty \frac{S}{1 + S}, \tag{1}$$

where R_∞ is the asymptotic rate at high intensity and $S = I/I_{\text{sat}}$, with I being the peak intensity of the excitation light incident on the sample and I_{sat} being the saturation intensity. These two fits gave saturation intensities $I_{\text{sat}}^{\text{dir}}$ = 90(8) kW/cm^2 and $I_{\text{sat}}^{\text{grat}}$ = 104(10) kW/cm^2 for the direct and grating collections, respectively, which are in good agreement with each other. The maximum photon rates were different, with values of R_∞^{dir} = 160(6) kcounts/s and R_∞^{grat} = 96(3) kcounts/s, because of the different collection efficiencies. The grating coupler on the right gave a count rate 10 times lower. We do not think this was due to a fabrication imperfection because the throughput of this device was similar to that of the others on the same substrate, and we have simulated different molecule positions on the device and found no asymmetry in emission. The more likely explanation is that the surface patterning of the gold, or imperfections in the anthracene crystal, favored emission into one direction over the other. The pulsed laser at 781 nm was then used to determine the decay time of the excited molecule. The semilog plot in Fig. 3(e) shows the measured probability distribution of delay times t between excitation of the molecule and detection of a photon, after correcting for the background count rate. A fit using the function $Ae^{-t/\tau}$ gave the lifetime of the excited state of the molecule as τ = 2.74(2) ns. This is slightly shorter than the expected 3–6 ns for DBT in bulk anthracene crystals,[2,3,26–28] but is within the range of expected lifetimes for similar DBT molecules covered with anthracene using a supersaturated vapor growth on glass (see supplementary material, Fig. S2). This lifetime suggests that the device does not introduce new
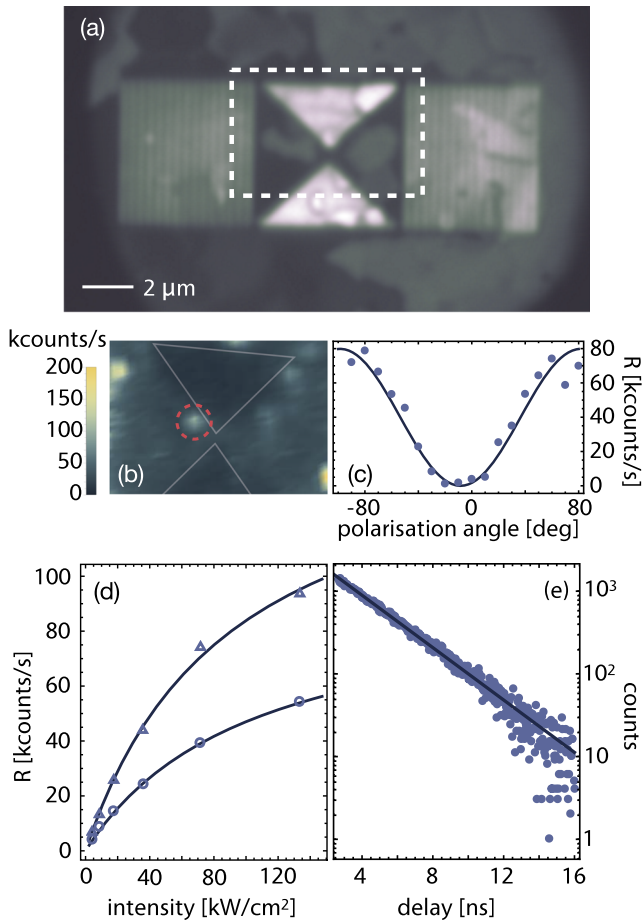
FIG. 3. (a) White-light image of a HGPW showing input/output grating couplers and anthracene crystals on the surface. (b) Molecule fluorescence from the dashed box in (a). The gray lines outline the edges of the gold. (c) Collected count rate as a function of laser polarization for the molecule outlined by the dashed red circle in (b). (d) Saturation curves for that molecule. Data points show count rates collected from the confocal microscope (triangles) and from a grating coupler (circles). The data are well fitted by the nonlinear function [Eq. (1)] (solid lines). (e) Pulsed laser measurement of the excited state lifetime of the same molecule.

nonradiative decay paths, and shows, as expected, that the radiative decay rate is not significantly enhanced by the plasmonic structure for this gap width (see supplementary material, Fig. S6).

To confirm that this was indeed a single molecule, we measured the second-order correlation function $g^{(2)}(\tau)$ for the emitted light, while exciting the molecule at a saturation level $S \approx 1$. As a single molecule can only emit one photon at a time, we expect that $g^{(2)}(0) = 0$ in the ideal case.[29] To determine $g^{(2)}(\tau)$ for the fluorescence collected directly from the molecule, a 50:50 multimode fiber splitter [Fig. 2(c)] divided the light between two avalanche photodiodes and a time correlating card recorded the histogram of start–stop intervals in the standard way. Figure 4(a) shows the data points, together with a fit to the function[28]

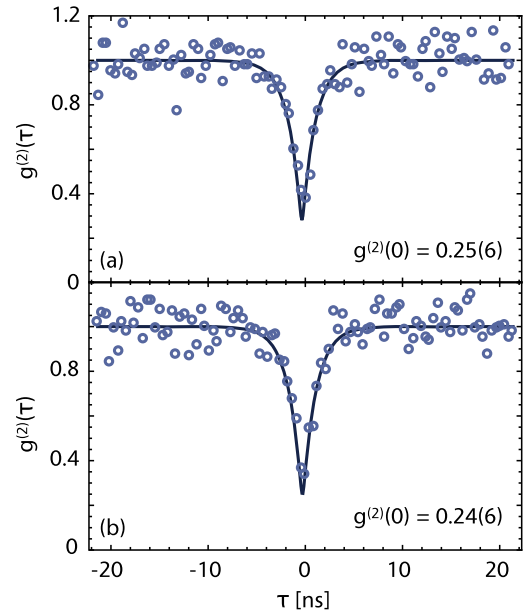$$g^{(2)}(\tau) = 1 - B e^{-(1+S)\frac{t}{\tau}}, \qquad (2)$$

FIG. 4. Correlation functions $g^{(2)}(\tau)$ for the DBT fluorescence. (a) Autocorrelation of light collected directly from the molecule through the confocal microscope after beam splitting. (b) Cross-correlation of light collected from the left grating and from the confocal microscope. Dots show data. Solid curves are fits using Eq. (2). In both cases, $g^{(2)}(0)$ is well below 0.5 showing clear antibunching.

where $B = 1 - g^{(2)}(0)$ is the only free parameter. This $g^{(2)}(\tau)$ exhibits clear antibunching, with the fit giving $g^{(2)}(0) = 0.25(6)$. Next, we removed the fiber splitter and instead measured the time correlation between the light from the molecule and that collected from the grating. This gave the $g^{(2)}(\tau)$ in Fig. 4(b), where $g^{(2)}(0) = 0.24(6)$. The two values of $g^{(2)}(0)$ agree. The fact that $g^{(2)}(0) < 0.5$ without any correction (e.g., for background counts, dark counts, or possible nearby emitters) signifies that we were indeed collecting fluorescence predominantly from a single molecule in both cases. After convolving Eq. (2) with the Gaussian instrument response function due to a detector timing jitter (standard deviation of 455 ps), both data sets gave $g^{(2)}(0) = 0.20(2)$, a value that is consistent with the signal-to-background ratio found in each case.

IV. DEDUCING THE COUPLING EFFICIENCY

We use the detected fluorescence rate to estimate the coupling factor β, defined as the fraction of emitted photons coupled into the waveguide,

$$\beta = \frac{\Gamma_{wg}}{\Gamma_{tot}}, \qquad (3)$$

where Γ_{wg} is the rate at which the molecule emits photons into the waveguide and Γ_{tot} is its total emission rate, which we assume to be purely radiative. The rate at which photons are detected from the grating is $R_{grat} = \Gamma_{wg}\eta_{grat}$, where η_{grat} is the efficiency for coupling light out from the waveguide, collecting it, and detecting it using the APD. We can further write $R_{grat} = R_\infty^{grat} S/(1 + S)$, where R_∞^{grat} is the fully saturated rate detected from the grating. Similarly, the total emission rate can be written as $\Gamma_{tot} = \alpha \Gamma_1 S/(1 + S)$, where $\Gamma_1 = 1/\tau$,

α is the maximum excitation probability for the pump wavelength used[30] and lies between 0.5 and 1, and S is once again the saturation parameter. In the limit of large S, this tends to α/τ. Thus, the coupling factor β is given by

$$\beta = \frac{\tau}{\alpha} \frac{R_\infty^{\text{grat}}}{\eta_{\text{grat}}}. \tag{4}$$

We have measured τ and R_∞^{grat} (see above), and for room-temperature DBT excited at 780 nm, we know[30] that $\alpha = 0.555(10)$. This leaves us needing to assess η_{grat}.

At room temperature, the DBT molecule emits photons over ~20 THz wide frequency range.[30] This is broad enough that η_{grat} has to be determined by convolving the emission spectrum with the frequency-dependent outcoupling/collection/detection efficiency. In separate experiments (see supplementary material, Fig. S4), we have measured the frequency-dependent output coupling from the waveguide through the grating. With a peak value of 10% at 800 nm, dropping to 2% at 765 nm and 830 nm, this is the main loss-factor contributing to η_{grat}. We have also accounted for the frequency-dependent transmission of all the other optical elements (see supplementary material, Fig. S5). The result is $\eta_{\text{wg}} = 4.1(5) \times 10^{-3}$, which leads to a coupling efficiency of the molecule to the waveguide of $\beta = 11.6(1.5)\%$. It should be noted that if nonradiative decays were to contribute to the measurement of τ, then Γ_{tot} would be overestimated and our measurement would correspond to a lower bound on the coupling efficiency. We could have chosen to calculate the coupling efficiency by comparing the number of photons detected via the grating to those detected directly through the confocal microscope, after correcting both for their collection efficiencies. We chose not to do this as the collection efficiency through the confocal arm of the setup varies broadly by up to 50% due to the unknown radiation pattern of the DBT molecule, depending on its position within the anthracene crystal and relative to the interfaces of the chip layers. We find efficiencies between 5×10^{-4} and 1.2×10^{-3}, and recently[30] measured $1.03(2) \times 10^{-3}$. Here, we find a confocal collection efficiency of $\eta_{\text{cfcl}} = (\tau R_{\text{cfcl}})/\alpha = 8(1) \times 10^{-4}$ which is within the expected range and suggests that nonradiative decay paths are not introduced by the presence of the gold. The coupling efficiency agrees well with finite difference time domain simulations; while these did not show the same asymmetry between left and right grating emission, they resulted in a total coupling efficiency to the waveguide mode of $\beta_{\text{sim}} = 11.5\%$ (see supplementary material, Fig. S6). Other experiments have observed similarly high coupling to dielectric waveguides,[4,13,31] but the use of plasmonics in our case opens the possibility of much stronger coupling in the future.

V. SUMMARY AND FUTURE PROSPECTS

We have observed the coupling of a single DBT molecule to a HGPW made from a multilayer dielectric slab patterned with gold structures. Measurements of the molecule itself gave values for the orientation, excited state lifetime, and saturation intensity, and confirmed through the second-order correlation function $g^{(2)}(\tau)$ of the emitted light that this was a single molecule. We also detected the light coupled out of the waveguide by a grating and measured the cross-correlation of this light with that observed at the molecule. This showed that the light at the grating was indeed emitted by the molecule. The photon count rate detected at the grating was used to infer the efficiency β with which the molecule radiated photons into the guide. These measurements were made at room temperature, where phonon-induced dephasing of the optical dipole[28,30] makes the photons spectrally broad. Such photons can be useful for communication and imaging, but not for applications that require quantum interference such as linear optical quantum computing or quantum simulation. In the future, we will look for molecules coupled to HGPW at liquid helium temperatures, where decoherence should be minimized so the spectrum can exhibit a Fourier-limited spectral width. Moreover, the reduced absorption linewidth will allow us to increase the concentration of DBT molecules by several orders of magnitude, increasing the probability of finding a molecule in a favorable position.

These measurements were made on a single device with a gold gap width of 200 nm, which is not expected to give a large enhancement of the photon emission rate. We plan to look for molecules coupled to guides with smaller gap sizes where the coupling should be strongly enhanced. One of the main limitations in our device was the low contrast of the refractive index between the titanium dioxide and the silica substrate. To improve this, we have simulated the case of gallium phosphide (GaP) on silica, as it presents a refractive index comparable to silicon and shows low losses in the near-infrared.[32] Modifying our structure[22] with a thinner spacing layer to retain mode hybridization, we have found that a total coupling efficiency higher than 50% can be achieved by placing a DBT molecule in a 500 nm long waveguide with a gap width of 100 nm.

Finally, in the future it should be possible to use similar plasmonic structures to shift the waveguide mode adiabatically in and out of low-loss dielectric ridge waveguides, creating regions of strong light-matter interaction at precise locations in a low-loss integrated photonic network.

SUPPLEMENTARY MATERIAL

See supplementary material for a more detailed experimental setup, DBT lifetime measurements, coupling to a longer HGPW, detailed coupling calculations, and finite-difference time-domain simulation results. All data is available upon reasonable request to the corresponding author.

ACKNOWLEDGMENTS

REFERENCES

[1] I. Aharonovich, D. Englund, and M. Toth, Nat. Photonics **10**, 631 (2016).

[2] A. A. L. Nicolet, P. Bordat, C. Hofmann, M. A. Kol'chenko, B. Kozankiewicz, R. Brown, and M. Orrit, ChemPhysChem **8**, 1215 (2007).

[3] J.-B. Trebbia, H. Ruf, P. Tamarat, and B. Lounis, Opt. Express **17**, 023986 (2009).

[4] S. Faez, P. Türschmann, H. R. Haakh, S. Götzinger, and V. Sandoghdar, Phys. Rev. Lett. **113**, 213601 (2014); e-print arXiv:1407.2846.

[5] D. Wang, H. Kelkar, D. Martin-Cano, T. Utikal, S. Götzinger, and V. Sandoghdar, Phys. Rev. X **7**, 021014 (2017); e-print arXiv:1612.05007.

[6] P. Tamarat, A. Maali, B. Lounis, and M. Orrit, J. Phys. Chem. A **104**, 1 (2000).

[7] M. D. Eisaman, J. Fan, A. Migdall, and S. V. Polyakov, Rev. Sci. Instrum. **82**, 071101 (2011).

[8] B. J. M. Hausmann, T. M. Babinec, J. T. Choy, J. S. Hodges, S. Hong, I. Bulu, A. Yacoby, M. D. Lukin, and M. Lončar, New J. Phys. **13**, 045004 (2011).

[9] X. Ding, Y. He, Z.-C. Duan, N. Gregersen, M.-C. Chen, S. Unsleber, S. Maier, C. Schneider, M. Kamp, S. Höfling, C.-Y. Lu, and J.-W. Pan, Phys. Rev. Lett. **116**, 020401 (2016); e-print arXiv:1601.00284.

[10] N. Somaschi, V. Giesz, L. De Santis, J. C. Loredo, M. P. Almeida, G. Hornecker, S. L. Portalupi, T. Grange, C. Antón, J. Demory, C. Gómez, I. Sagnes, N. D. Lanzillotti-Kimura, A. Lemaître, A. Auffèves, A. G. White, L. Lanco, and P. Senellart, Nat. Photonics **10**, 340 (2016).

[11] J. Hwang and E. A. Hinds, New J. Phys. **13**, 085009 (2011).

[12] C. Polisseni, K. D. Major, S. Boissier, S. Grandi, A. S. Clark, and E. A. Hinds, Opt. Express **24**, 5615 (2016).

[13] P. Türschmann, N. Rotenberg, J. Renger, I. Harder, O. Lohse, T. Utikal, S. Götzinger, and V. Sandoghdar, Nano Lett. **17**, 4941 (2017).

[14] Q. Xu, V. R. Almeida, R. R. Panepucci, and M. Lipson, Opt. Lett. **29**, 1626 (2004).

[15] J. T. Robinson, C. Manolatou, L. Chen, and M. Lipson, Phys. Rev. Lett. **95**, 143901 (2005).

[16] C. A. Barrios, B. Sánchez, K. B. Gylfason, A. Griol, H. Sohlström, M. Holgado, and R. Casquel, Opt. Express **15**, 6846 (2007).

[17] F. B. C. Dieleman, "Quantum properties of plasmonic waveguides," Ph.D. thesis, Imperial College London, 2017.

[18] H. Siampour, S. Kumar, and S. I. Bozhevolnyi, ACS Photonics **4**, 1879 (2017).

[19] K. G. Lee, X. W. Chen, H. Eghlidi, P. Kukura, R. Lettow, A. Renn, V. Sandoghdar, and S. Götzinger, Nat. Photonics **5**, 166 (2011).

[20] S. Checcucci, P. E. Lombardi, S. Rizvi, F. Sgrignuoli, N. Gruhler, F. B. Dieleman, F. S. Cataliotti, W. H. Pernice, M. Agio, and C. Toninelli, Light: Sci. Appl. **6**, e16245 (2017).

[21] L. Lafone, T. P. H. Sidiropoulos, and R. F. Oulton, Opt. Lett. **39**, 4356 (2014).

[22] M. P. Nielsen, L. Lafone, A. Rakovich, T. P. H. Sidiropoulos, M. Rahmani, S. A. Maier, and R. F. Oulton, Nano Lett. **16**, 1410 (2016).

[23] M. P. Nielsen, X. Shi, P. Dichtl, S. A. Maier, and R. F. Oulton, Science **358**, 1179 (2017).

[24] N. B. Nguyen, M. P. Nielsen, L. Lafone, E. Clarke, P. Fry, and R. F. Oulton, Appl. Phys. Lett. **111**, 261107 (2017).

[25] B. Kozankiewicz and M. Orrit, Chem. Soc. Rev. **43**, 1029 (2014).

[26] K. D. Major, Y.-H. Lien, C. Polisseni, S. Grandi, K. W. Kho, A. S. Clark, J. Hwang, and E. A. Hinds, Rev. Sci. Instrum. **86**, 083106 (2015).

[27] C. Toninelli, K. Early, J. Bremi, A. Renn, S. Götzinger, and V. Sandoghdar, Opt. Express **18**, 6577 (2010).

[28] S. Grandi, K. D. Major, C. Polisseni, S. Boissier, A. S. Clark, and E. A. Hinds, Phys. Rev. A **94**, 063839 (2016).

[29] R. Loudon, *The Quantum Theory of Light*, 3rd ed. (Oxford Science Publications, 2000).

[30] R. Schofield, K. D. Major, S. Grandi, S. Boissier, E. A. Hinds, and A. S. Clark, J. Phys. Commun. **2**, 115027 (2018).

[31] P. Lombardi, A. P. Ovvyan, S. Pazzagli, G. Mazzamuto, G. Kewes, O. Neitzke, N. Gruhler, O. Benson, W. H. P. Pernice, F. S. Cataliotti, and C. Toninelli, ACS Photonics **5**, 126 (2018).

[32] K. Schneider, P. Welter, Y. Baumgartner, H. Hahn, L. Czornomaz, and P. Seidler, J. Lightwave Technol. **36**, 2994 (2018).